Journal of Molecular Structure 1238 (2021) 130344

Contents lists available at ScienceDirect

Journal of Molecular Structure

journal homepage: www.elsevier.com/locate/molstr

Specific features of structural, magnetic, Raman and Mössbauer: Properties of $La_{0.57}Nd_{0.10}Sr_{0.18}Ag_{0.15}FeO_3$ ferrite nanoparticules

F. Issaoui [a,*], H. Issaoui [b], E. Dhahri [b], Benilde F.O. Costa [c], Bernardo A. Nogueira [d], Rui Fausto [d]

[a] Research Unit Valorization and Optimization of Resource Exploitation, Faculty of Science and Technology of Sidi Bouzid, University of Kairouan, Sidibouzid, 9100, Tunisia
[b] Laboratoire de Physique Appliquée, Faculté des Sciences de Sfax, B.P 1171, Sfax 3000, Tunisia
[c] CFisUC, University of Coimbra, Department of Physics, P-3004-516 Coimbra, Portugal
[d] CQC, University of Coimbra, Department of Chemistry, P-3004-535 Coimbra, Portugal

ARTICLE INFO

Article history:
Received 16 January 2021
Revised 13 March 2021
Accepted 23 March 2021
Available online 6 April 2021

Keywords:
Solid-state synthesis
Ferrite nanoparticles
Magnetic properties
X-ray diffraction
Raman spectroscopy
Mössbauer spectroscopy

ABSTRACT

This article reports on a detailed study of the structural, spectroscopic and magnetic properties of $La_{0.57}Nd_{0.10}Sr_{0.18}Ag_{0.15}FeO_3$ (LNSAFO) ferrite nanoparticles, which were prepared using the solid state technique. The Rietveld analysis of the powder X-ray diffractograms indicated that the material crystalizes in an orthorhombic structure, Pnma space group. Scanning electron microscopy (SEM) measurements showed that all particles have almost spherical shapes, and are characterized by a distribution of relatively narrow particle sizes. The average diameter of the particles was estimated within the 25–45 nm range by three different methods (SEM, and from the XRD data using the Debye-Scherer and Williamson–Hall models).The elemental composition of the synthesized material has been investigated by energy dispersive spectroscopy (EDS), which confirmed the presence of all expected elements in stoichiometries matching those of the precursor oxides of the synthesized perovskite. Raman spectroscopy measurements revealed that the studied sample had a considerable degree of crystallinity, in agreement with the X-ray diffraction data. Finally, the magnetic properties of the studied compound have been investigated by studying the variation of the magnetization as a function of temperature in both the ZFC (zero field cooled) and FC (field cooled) modes. A blocking temperature (T_B) of around 100 K was observed.

Published by Elsevier B.V.

Highlights (for review)

- The SEM measurements showed that all particles have almost spherical shapes and are characterized by a distribution of relatively narrow particle size with an average diameter of about 55 nm.
- The Rietveld analysis of X-ray diffractograms indicated an orthorhombic structure.
- The variation of magnetization as a function of temperature in ZFC (zero field cooled) mode and FC (field cooled) mode. We notice the existence blocking temperature (T_B) at around 100 K.

1. Introduction

In recent years, the scientific community has been showing a growing interest in perovskite materials of general structure ABO_3, both for fundamental research and technological applications in the fields of electronics and sensors, as well as for their use as a cathode or electrolyte in a solid oxide fuel cell and as a catalyst for redox reactions (automotive catalyst) [1–5]. In particular, great effort has been made to obtain fundamental structural information on iron oxides of formula $LaFeO_3$ and its derivatives, and to measure the relevant properties for their practical applications (for example as sensors), including their optical and magnetic properties.

A favorable characteristic of this type of material is that it is relatively easy to modulate their physical properties by structural modifications, which include the nature and concentration of a dopant, as well as the doping site(s) [6–10]. Indeed, $LaFeO_3$ doped materials are known by their good optical and magnetic proprieties for applications in optoelectronics and spintronics [11–13]. Among the possible dopants, Sr and Nd(as a co-doping system) appear of interest, taking into account the improved properties resulting by $LaFeO_3$ doping with each one of these elements, which include better photocatalytic activity and sensing sensibility and selectivity, as well as improved efficiency for adsorption of gasses at active surfaces and oxidation capabilities [14–16]. In this article the synthesis, and structural, spectroscopic and mag-

* Corresponding author.
E-mail address: issawi_fatma@yahoo.fr (F. Issaoui).

https://doi.org/10.1016/j.molstruc.2021.130344
0022-2860/Published by Elsevier B.V.

netic characterization of the $LaFeO_3$ Sn/Nd co-doped derivative, $La_{0.57}Nd_{0.10}Sr_{0.18}Ag_{0.15}FeO_3$ (LNSAFO) are reported. As a whole, the obtained results contribute to a better understanding of the physicochemical properties of this material and their relationship with its structural aspects.

2. Experimental

2.1. Synthesis

The powder sample of LNSAFO was prepared using the solid-state reaction method in presence of air. The precursors (purity > 99.9%) used for the preparation of the compound were lanthanum oxide La_2O_3, neodymium oxideNd_2O_3, ironoxide FeO_3, strontium oxide SrO, and silver oxide Ag_2O, according to the reaction:

$$0.285La_2O_3 + 0.05Nd_2O_3 + 0.18SrO + 0.075Ag_2O + FeO_3 \rightarrow La_{0.57}Nd_{0.10}Sr_{0.18}Ag_{0.15}FeO_3 + 0.57\ O_2$$

The oxide precursors were intimately mixed in an agate mortar according to the desired stoichiometry, and ground for 30 min to obtain a homogeneous mixture. Then, the mixture was placed in platinum crucibles and baked at 700 °C for 48 h. The resulting material was then brought to a temperature of 1000 °C, interspersed with several cycles of grinding and annealing. This step made it possible to reduce the size of the grains and to homogenize the obtained powders, which were then put in the form of thin pellets and placed in the oven at a temperature of 1300 °C for 24 h.To properly estimate the better final annealing temperature, a series of experiments were carried out at temperatures ranging from 1200 to 1300 °C, demonstrated that, below 1300 °C, the final product is obtained as a single phase. The sample was finally cooled to ambient temperature by rapid quenching in air [17].

2.2. Characterization of the synthesized material

The phase purity, lattice structure and cell parameters of the synthesized compound were obtained by X-ray diffraction (XRD), using a Bruker 8D Advance X-ray powder diffractometer, working with CuKα_1 radiation (λ = 1.5406 Å), in the θ–2θ Bragg-Brentano geometry. The acquisition was performed in the 2θ range of 5–100°, with a step of 0.03° and an acquisition time for each step of 1 s. The XRD data were used to obtain the lattice parameters by means of Rietveld analysis [18], using the FULLPROF program [19]. Microstructure and grain sizes were observed using a TESCAN VEGA3 SBH scanning electron microscope (20 kV) equipped with an EDS detector BrukerXFlagh 410 M, which allows determination of the chemical elements present in the sample. For the analysis, a little amount of the powder of the compound was deposited on a carbon tape.

The Raman data were obtained, in the wavenumber range 80–1600 cm^{-1}, in a Raman micro-system (Horiba LabRam HR Evolution), equipped with a Synapse CCD detector, a high-stability BXFM open-space confocal microscope, and a 600 $gr.mm^{-1}$ grating, using 532 nm excitation. The laser power at the sample was approximately 17 mW, and the exposure time 30 s. A 50x objective lens was used. The final spectra are obtained by averaging of 60 scans.

The magnetic properties of the compounds, namely hysteretic cycles and FC-ZFC curves, were measured in a Vibrating Sample Magnetometer (VSM) with a cryogen-free DynaCool PPMS, operating at a vibration frequency of 40 Hz and amplitude of 2 mm in the central area of the coils. In order to undertake the analyses, the samples were placed in a Perspex rod-shaped sample holder. Additional magnetic measurements were done using a Faraday type magnetometer MANICS DSM8,between 2 and 300 K.

Mössbauer spectra were recorded at room temperature (RT) in a transmission geometry WissEL spectrometer, using a source of ^{57}Co in a Rh matrix with an activity of 10 mCi. The sample was in powder form and was put in a sample holder made of Perspex. The measurements were carried out in a spectrometer operating with a triangular velocity waveform. The spectral data were fitted by using the least squares method, with a set of Lorentzian lines, with the program NORMOS [20],which is distributed by WissEL GmbH. Isomer shifts are given relative to α–Fe measured at RT.

3. Results and discussion

3.1. Structural and microstructural properties

In order to identify the phases present in the sample and check their purity, an analysis by X-ray diffraction was performed. The X-ray diffractogram obtained at room temperature is shown in Fig. 1. It shows fine and intense lines, a sign of good crystallization without any trace of impurity. The Rietveld refinement shows an excellent agreement with the experimental data. The result of the refinement allows to conclude that our compound crystallizes in the orthorhombic structure, space group Pnma, with a = 5.5438, b = 7.5697 and c = 5.5845 Å.

The Goldschmidt's tolerance factor, t_G, was used as an additional indicator of the structure of the material. It is an indicator

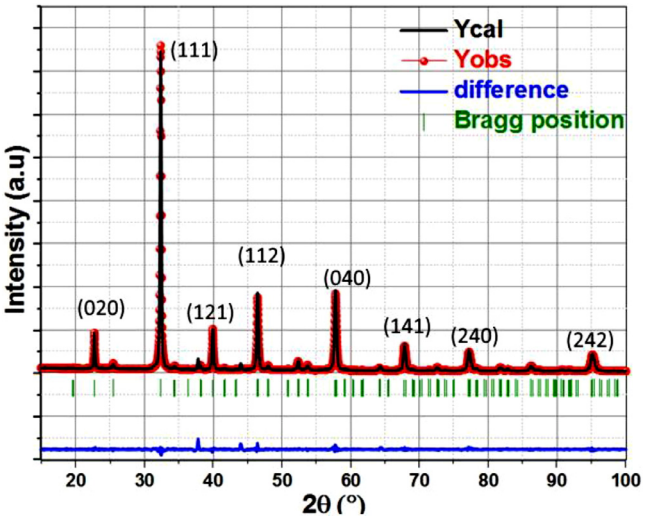

Fig. 1. Rietveld analysis of the XRD patterns of LNSAFO, and peak indexation.

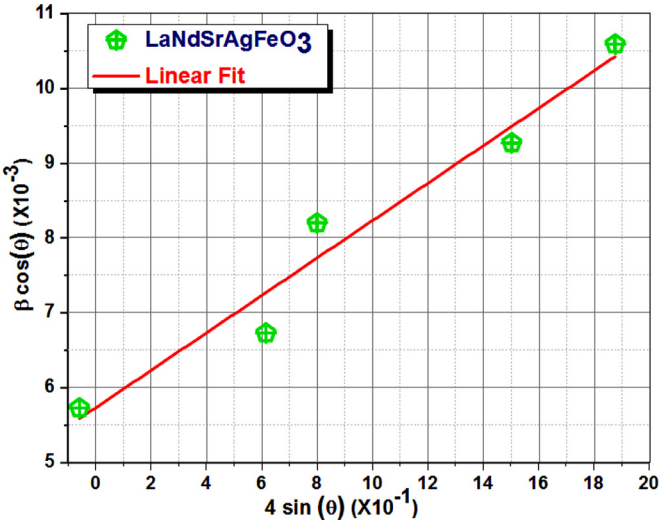

Fig. 2. Williamson–Hall plot for LNSAFO.

for the stability and distortion of the crystal structure and can be calculated from Eq. (1) [21],

$$t_G = \frac{r_A + r_O}{(r_B + r_O)\sqrt{2}} \quad (1)$$

where $r_A = r(La^{3+}, Nd^{3+}, Sr^{2+}, Ag^{+})$, $r_B = r(Fe^{3+})$ and r_O (O^{2-})are the ionic radii associated with the cations of the perovskite sites A and B and oxygen anion, respectively. For the studied compound, using the crystal ionic radii of O^{2-}, La^{3+}, Nd^{3+}, Sr^{2+}, Ag^{+}, Fe^{3+} and Fe^{2+} of 1.260, 1.216, 1.123, 1.320, 1.290, 0.640 and 0.750 Å [22]:

$$< r_A > = 0.57r\left(La^{3+}\right) + 0.1r\left(Nd^{3+}\right) + (0.33 - 0.15)r\left(Sr^{2+}\right) + 0.15r\left(Ag^{+}\right) = 1.236\text{Å}$$

$$< r_B > = 0.52r\left(Fe^{3+}\right) + (1 - 0.52)r\left(Fe^{2+}\right) = 0.6928\text{Å}$$

$$r_O = 1.260\ \text{Å}$$

so that t_G is 0.903, which stays within the range of values compatible with an orthorhombic structure (0.71–0.96 [21,23]).

The average crystallite size was determined from the most intense peak of the XRD diffractogram using the Debye–Scherrer formula:

$$D_{SC} = \frac{0.9 \times \lambda}{\beta \times cos\theta} \quad (2)$$

where λ is the used wavelength, θ the Bragg angle of the most intense peak and β the width at half height of this peak. The obtained mean value of the Debye-Scherer crystallite size (D_{SC}) for LNSAFO was 25 nm, which confirmed the nanometric size of the particles of the compound.

The Williamson–Hall method is another method to determine crystallite sizes [24], and was also used in the present study. It is expressed as:

$$\beta \cos\theta = \frac{k\lambda}{D} + 4\varepsilon \sin\theta \quad (3)$$

The Williamson–Hall crystallite size (D_{W-H}) and the microstrain, ε, can be obtained from the y-intercept and the slope, respectively, of the linearly fitted data, (β cosθ) as a function of 4sinθ, amounting to 37 nm and 0.0004.It is worth noting that the crystallite size calculated by the Williamson–Hall method is slightly higher than that calculated using the Debye–Scherrer equation, because the broadening effect due to the microstrain is completely excluded in this latter [25].

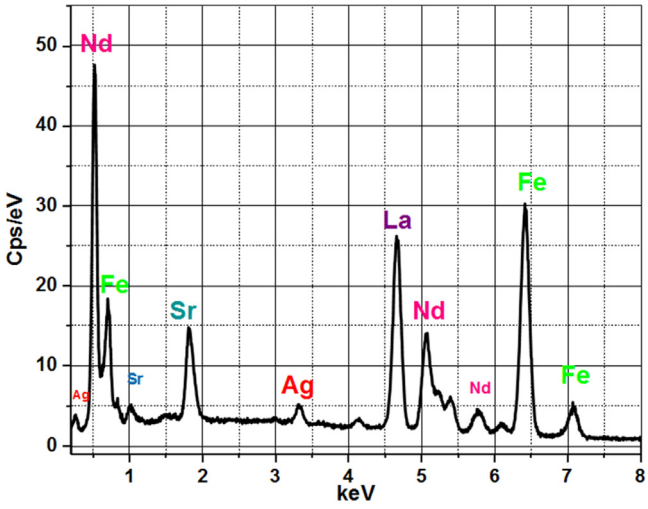

Fig. 4. EDS spectrum of LNSAFO.

The structural study by X-ray diffraction was supplemented by an analysis of the surface morphology using scanning electron microscopy (SEM). As it can be seen in Fig. 3b, a non-uniform grain distribution in the samples was observed. Furthermore, the grains have a quasi-spherical shape. The grain size distribution was obtained using the Image-J software, and compiled in the histogram shown in Fig. 3a, the average value obtained by this approach being ca. 45 nm, i.e., slightly larger than the values obtained from the XRD data using the Debye-Scherer and Williamson–Hall models.

The elemental composition of the sample was analyzed using energy dispersive spectroscopy (EDS). The results are shown in Fig. 4, and also in Table 1 where the elements' abundances in the sample (percent weights) are given. It is worth mentioning the very good agreement between the EDS determined composition

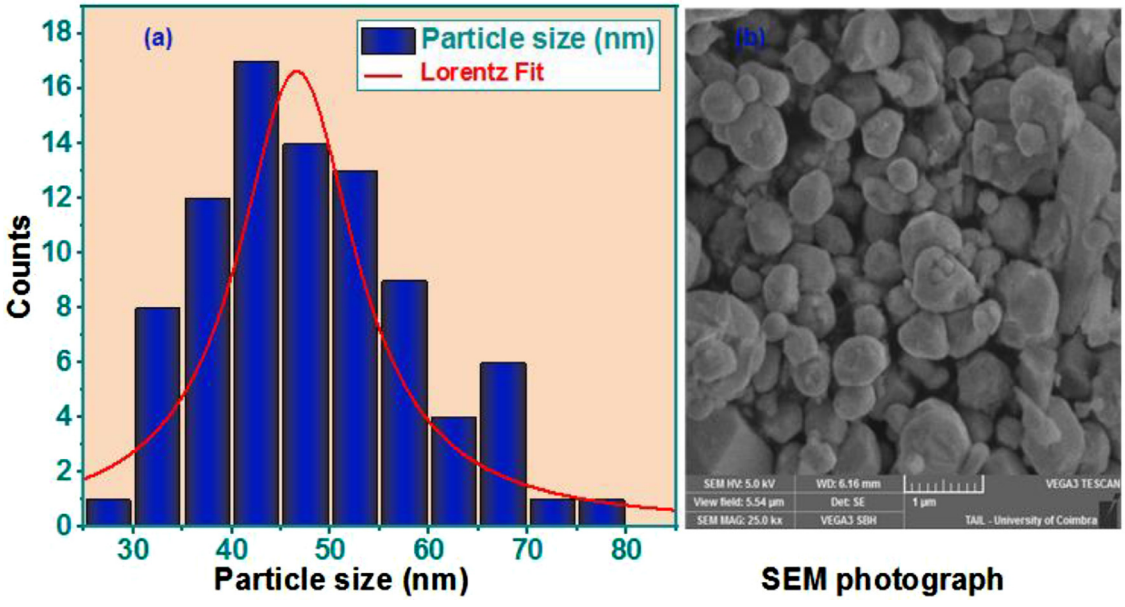

Fig. 3. Size distribution histogram **(a)**, and SEM micrograph **(b)** for LNSAFO.

Table 1
Elemental composition of LNSAFO as determined by EDS.

Element	Weight (%)	Atomic (%)
Oxygen	18.88	56.62
Iron	25.72	22.10
Strontium	8.25	4.52
Silver	0.49	0.22
Lanthanum	37.81	13.06
Neodymium	7.89	2.62

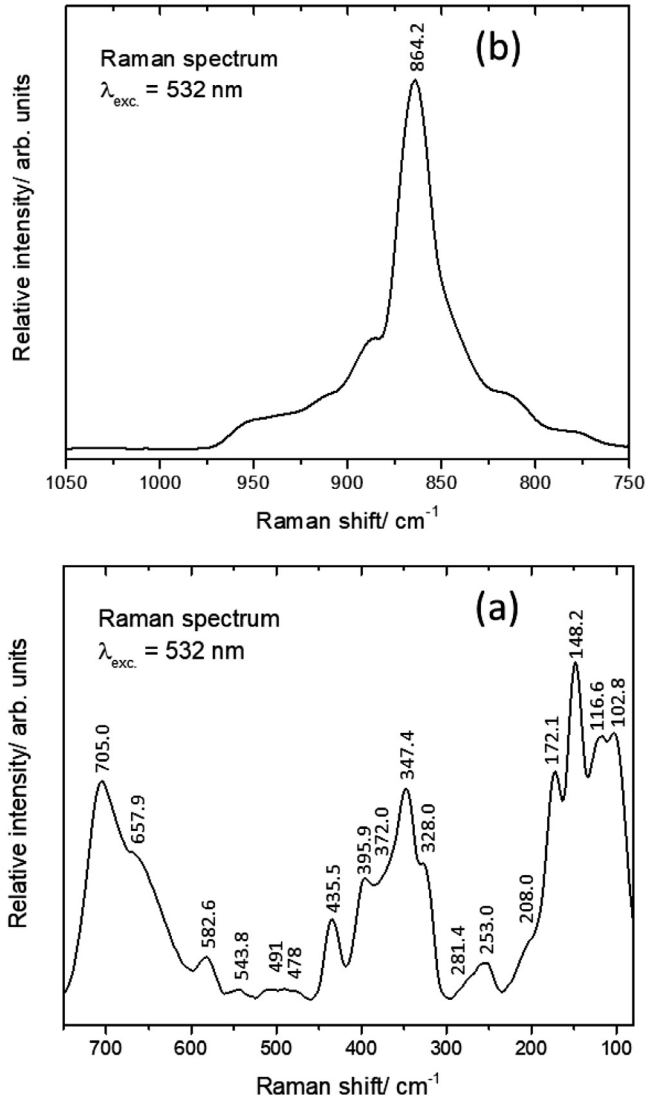

Fig. 5. Room temperature Raman spectrum of LNSAFO, in the 90–750 cm^{-1} (**a**) and 750–1050 cm^{-1}(**b**) spectral ranges.

and the expected stoichiometry of the starting materials used for the preparation of sample.

3.2. Raman spectroscopy results

The Raman spectrum of the studied material was registered at room temperature using the conditions provided in the Experimental section. No pre-processing of the sample was done. The obtained spectrum, in the 90–750 and 750–1050 cm^{-1} ranges, is shown in Fig. 5.

In the 90–750 cm^{-1}range (Fig. 5a), the characteristic Raman bands of the $LaFeO_3$ structure dominate the spectrum. These bands are observed at 102.8, 148.2 and 172.1 cm^{-1}, which are ascribable to La-sites vibrations [26–29], as well as at 253.0, 281.4, 395.9, 435.5 and 657.9 cm^{-1}, which originate in the Fe-sites. The frequencies of these bands match well the previously reported values (110, 145 and 170 cm^{-1}, in the case of the La-sites related vibrations [26–29], and 255, 285, 400, 430 and 640 cm^{-1} for the Fe-sites [27–29]). The 395.9 and 435.5 cm^{-1} bands are ascribable to O-Fe-O bending vibrations, while that observed at 657.9 cm^{-1} is assigned to the O-Fe-O stretching modes [27–31]. Two additional bands, observed at 582.6 and 705.0 cm^{-1} are much probably also due to the O–Fe–O stretching vibrations, shifted in frequency relative to that observed for the pristine $LaFeO_3$ because of the structural distortions induced by the doping of ions of different sizes in the studied material. The remaining bands are not present in the Raman spectrum of pure $LaFeO_3$ and shall be assigned to vibrational modes which involve the dopant atoms. The two bands observed at 116.6 and 208.0 cm^{-1} are here assigned to vibrations involving the Sr-O moiety. The higher frequency band shall also receive contribution from vibrations associated with the Ag dopant, since in the Raman spectra of AgO films a band has been observed at 217 cm^{-1}[32]. In the spectrum of this last material, other bands were observed at 302, 379, 429 and 487 cm^{-1} [32], which are here put in correspondence with the bands at 328.0, 372.0, 478 and 491 cm^{-1}, respectively, observed in the spectrum of the presently studied perovskite. Finally, the bands observed at 347.4 and 543.8 cm^{-1} are tentatively assigned to vibrations involving the Nd dopant atoms, since in the Raman spectrum of NdO bands are present at 413 and 630 cm^{-1} [33], appearing at slightly different wavenumber values in this latter material when compared to their position in the Raman spectrum of LNSAFO due to the different structural environments.

Above 750 cm^{-1}, no bands are observed in the Raman spectrum of the studied material, with the exception of that at 864.2 cm^{-1}, which exhibits a series of lower intensity satellite bands within the 775–975 cm^{-1} spectral range (Fig. 5b), which shall be ascribed to oxygen species(mainly peroxide anion, O_2^{-2}[34]) adsorbed onto the surface of the sample. Very interestingly, this band shows a narrower profile compared to the analogous feature observed previously for other similar materials [27,35]and a somewhat higher frequency, which points to a less tightened adsorption in the present case, possibly taking place at strongly preferred sites.

It is also interesting to note that the general profile of the Raman spectrum of the studied material is characterized by relatively narrow bands, which is an indication of a considerable degree of crystallinity of the sample. This result in agreement with the data here reported, obtained from X-ray diffraction measurements.

3.3. Magnetic measurements

The magnetization curves M(*T*)-ZFC and M(*T*)-FC are shown in Fig. 6 and have a common part, for the highest temperatures, in which the variations of the magnetization with the temperature are superimposed and reversible; that is, heating and cooling does not affect the magnetization. On the other hand, at low temperatures, the behavior is irreversible with a large divergence between M(*T*)-ZFC and M(*T*)-FC. The temperature corresponding to the separation between the two curves is called thermomagnetic irreversibility temperature or blocking temperature, noted T_{irr} or T_B, which for LNSAFO is approximately equal to 100 K.The irreversibility between M(*T*)-ZFC and M(*T*)-FC may therefore be due to the trapping of the walls of low-field domains, as has been observed for manganites [36].

The study of the variation of the magnetization as a function of the magnetic field for our material (Fig. 7) shows that the saturation magnetization decreases with increasing temperature and shows a clear hysteresis. Indeed, the hysteresis loop shows the existence of a coercive field Hc (0.06T) and a moderate remnant mag-

Table 2
Mössbauer parameters resulting from the fit to the spectrum shown in Fig. 8.

δ (mm/s)	2ε/QS (mm/s)	B(T)	Γ (mm/s)	%	coordination	site
0.34(1)	0.065(1)	48.3(1)	0.61(1)	27.5	Sextet Fe^{3+}	Site 1
0.36(1)	0.070(1)	44.3(1)	0.82(1)	27.0	Sextet Fe^{3+}	Site 2
0.29(1)	−0.090(1)	37.7(1)	1.61(1)	39.0	Sextet Fe^{3+}	Site 3
0.34(1)	2.220(1)	–	0.30(1)	4.5	Doublet Fe^{3+}	Site 4
1.69(1)	1.790(1)	–	0.45(1)	2.0	Doublet Fe^{2+}	Site 5

δ-isomer shift, 2ε/QS- quadrupole splitting, B-hyperfine magnetic field, Γ- line width at half maximum,%- site percentage. Isomer shifts are given relatively to α-Fe at R*T*.

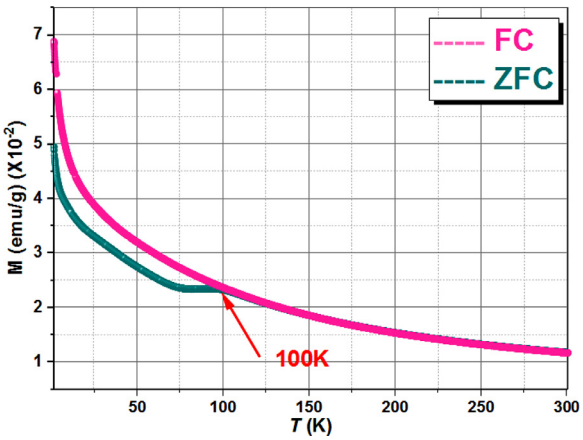

Fig. 6. M-*T* curves carried out with zero-field-cooling (ZFC) and field-cooling (FC) modes of LNSAFO.

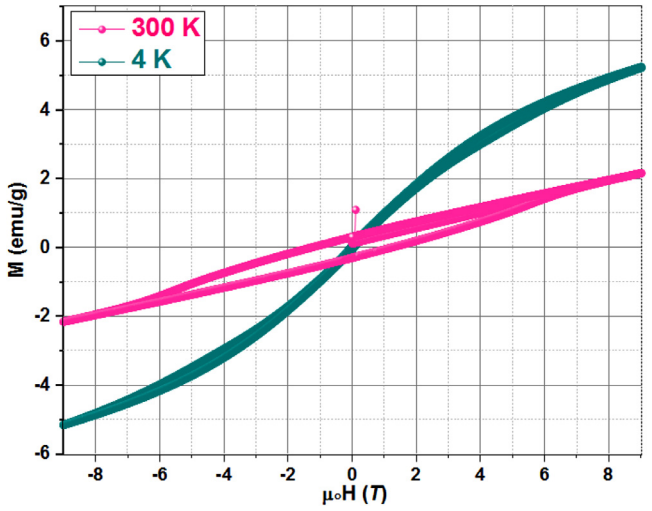

Fig. 7. Hysteresis loop for LNSAFO at 300 and 4 K.

netization Mr (0.45 $emug^{-1}$), in addition to a magnetization component which does not reach saturation even for a high magnetic field. This hysteresis loop indicates a strong antiferromagnetism. A low hysteresis is observed for $T = 4$ K and, together with the fact that the values of Hc and Mr are both very low, suggest a superparamagnetic behavior at low temperatures.

3.4. Mössbauer spectroscopy results

In order to investigate the iron valence states, we performed Mössbauer spectrometry measurements on the sample. The spectrum, taken at room temperature, is displayed in Fig. 8 and the hyperfine parameters that result from the fitting procedure are shown in Table 2. The spectrum was fitted with three sextets and

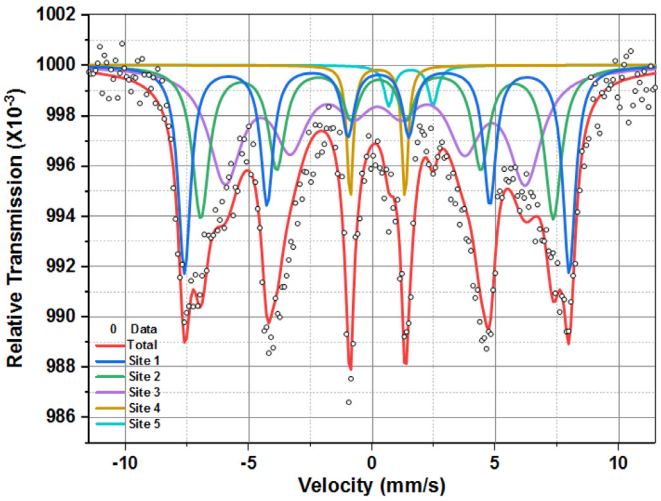

Fig. 8. Room temperature Mossbauer spectrum of LNSAFO.

two doublets. The existence of three sextets in doped $LaFeO_3$ compounds is due to non-equivalent positions of Fe^{3+}ions that arise from a weak distortion of the octahedral oxygen environment, as explained by Russo et al. [37]. The hyperfine magnetic fields are lower than the ones usually obtained for doped $LaFeO_3$ compounds, e.g. [8,27,35].. The linewidths of the sextets are large, being in accordance with a distortion of iron sites and also with a distribution of nanoparticles sizes. The doublets (Fe^{3+} and Fe^{2+}) are present in tiny concentrations and can be due to superparamagnetism.

4. Conclusion

The structural, spectroscopic and magnetic properties characterization of LNSAFO ferrite nanoparticles was undertaking by the conjugated use of different techniques. The synthesis of the compound by the solid state technique, the elemental composition of the synthesized sample, as obtained by energy dispersive spectroscopy, confirming the presence of all expected elements and in the expected percentages.

The Rietveld analysis of the powder XRD data indicated that the material crystalizes in an orthorhombic structure, Pnma space group, a result that receives further support from the obtained Goldschmidt's tolerance factor ($t_G = 0.88$), which falls within the range of values of this parameter for an orthorhombicstructure.

Scanning electron microscopy images showed that all particles are approximately spherical and have a relatively narrow size distribution, with an average diameter of about 45 nm (values slightly smaller were obtained from the XRD data using the Debye-Scherrer and Williamson–Hall model: 25 and 37 nm, respectively), while Raman spectroscopy measurements revealed that the sample had a considerable degree of crystallinity (in agreement with the XRD data).

The magnetization of the compound was investigated as a function of temperature in both the zero field cooled field cooled modes, allowing to find a blocking temperature at around 100 K.

Declaration of Competing Interest

None.

Acknowledgements

This work was supported by funds from (FCT – Fundaçãopara a Ciência e a Tecnologia, I.D., Portugal) provided within the project UID/04564/2020. Accesses to TAIL-UC under LaserLab Coimbra, funded under PProjectsQREN-Mais Centro ICT_2009_02_012_1890 and ROTEIRO/0152/2013, respectively, are also gratefully acknowledged. R.F. and B. A. N. acknowledge financial support from the FCT to CQC (Projects UIDB/00313/2020 and UIDP/00313/2020).

References

[1] R. Abazari, S. Sanati, Superlatt. Microstruct. 64 (2013) 148.
[2] G. Martinelli, M.C. Carotta, M. Ferroni, Y. Sadaoka, E. Traversa, Sens. Actuat.B-Chem. 55 (1999) 99.
[3] H. Saoudi, A. Benali, M. Bejar, E. Dhahri, T. Fiorido, K. Aguir, R. Hayn, J. Alloys Compd. 731 (2018) 655.
[4] K. Dumaisnil, D. Fasquelle, M. Mascot, A. Rolle, P. Roussel, S. Minaud, R.-N.Vannier B.Duponchel, J.-C. Carru, Thin Sol. Films 553 (2014) 89.
[5] R.J.H. Voorhoeve, J.P. Remeika, L.E. Trimble, A.S. Cooper, F.J. DiSalvo, P.K. Gallagher, J. Sol. State Chem. 14 (1975) 395.
[6] H. Issaoui, A. Benali, M. Bejar, E. Dhahri, B.F.O. Costa, M.P.F. Graca, M.A. Valente, RSC Adv. 10 (2020) 16132.
[7] H. Wu, Z. Xia, X. Zhang, S. Huang, M. Wei, F. Yang, Y. Song, G. Xiao, Z. Ouyang, Z. Wang, Ceram. Intern. 44 (2018) 146.
[8] H. Issaoui, B. Adel, M. Bejar, E. Dhahri, R.F. Santos, B.F.O. Costa, New J. Chem. 44 (2020) 9813.
[9] A.S. Mahapatra, A. Mitra, A. Mallick, M. Ghosh, P.K. Chakrabarti, Mater. Lett. 169 (2016) 160.
[10] N. Karthikeyan, R.R. Kumar, G. Jaiganesh, K. Sivakumar, Physica B 529 (2018) 1.
[11] Q. Yao, C. Tian, Z. Lu, J. Wang, H. Zhou, G. Ra, Ceram. Intern. 46 (2020) 20472.
[12] B. Kucharczyk, J. Winiarski, I. Szczygieł, K. Adamska, Ind. Eng. Chem. Res. 59 (2020) 16603.
[13] S. Tariq, A.A. Mubarak, F. Hamioud, M. Musa Saad, H.-E.S. Zahra, B. Kanwal, Q. Afzal, J. Alloys Comp. 831 (2020) 154600.
[14] M. Kaewpanha, T. Suriwong, W. Wamae, P. Nunocha, J. Phys.Conf. Ser. 1259 (2019) 012017.
[15] Y. Peng, W. Si, J. Li, J. Crittenden, J. Hao, Catal. Sci. Technol. 5 (2015) 2478.
[16] H. Sabeeh, S. Musaddiq, M. Shahid, M.A. Khan, M. Sher, M.F. Warsi, Mat. Res. Express 5 (2018) 065062.
[17] W. Boujelben, A. Cheikh-Rouhou, M. Ellouze, J.C. Joubert, Phase Transit. 71 (2000) 127.
[18] R.A. Young, The Rietveld Method, Oxford University Press, New York, 1993.
[19] J. Rodrigues-Carvajal, FULLPROF: A Rietveld Refinement and Pattern Matching-analysis Program, CEA-CNRS, Paris, France, 2000.
[20] R. Brand, Nucl. Inst. Meth. Phys. Res. B 28 (1987) 398.
[21] J.B. Goodenough, Phys. Rev. 100 (1955) 564.
[22] https://en.wikipedia.org/wiki/Ionic_radius, assessed on July 2020.
[23] https://en.wikipedia.org/wiki/Goldschmidt_tolerance_factor, assessed on July 2020.
[24] H. Issaoui, A. Benali, M. Bejar, E. Dhahri, M.P.F. Graca, M.A. Valente, B.F.O. Costa, Chem. Phys. Lett 731 (2019) 136588.
[25] P. Sherrer, Goett. Nachricht 2 (1918) 98.
[26] D. Triyono, H. Laysan, Mat. Sci. Eng. 496 (2019) 012045.
[27] M. Popa, J. Franti, M. Kakihana, Sol. State Ionn. 154/155 (2002) 135.
[28] A. Benali, M. Bejar, E. Dhahri, M. Sajieddine, M.P.F. Graça, M.A. Valente, Mat. Chem. Phys. 149/150 (2014) 467.
[29] Y. Wang, J. Zhu, L. Zhang, X. Yang, L. Lude, X. Wang, Mat. Lett. 60 (2006) 1767.
[30] S.M.A. Kader, D.E.J. Ruth, M.V.G. Babu, M. Muneeswaran, N.V. Giridharan, B. Sundarakannan, Ceram. Intern. 43 (2017) 15544.
[31] J. Geurts, S. Rau, W. Richter, F.J. Schmitte, Thin Sol. Films 121 (1984) 217.
[32] N.R.C. Raju, K.J. Kumar, A. Subrahmanyam, API Conf. Proc 1267 (2010) 1005.
[33] R. Yuvakkumar, S.I. Ho, J. Sol-Gel Sci. Technol. 73 (2015) 511.
[34] Y.M. Choi, H. Abernathy, H.-.T. Chen, M.C. Lin, M. Liu, Chem. Phys. (7) (2006) 1957.
[35] H. Issaoui, A. Benali, M. Bejar, E. Dhahri, R.F. Santos, N. Kuş, B.A. Nogueira, R. Fausto, B.F.O. Costa, J. Supercond. Novel Magnet. 32 (2019) 1571.
[36] B.D. Cullity, Introduction to Magnetic Material, Addison-Wesley, New York, USA, 1972.
[37] U. Russo, L. Nodari, M. Faticanti, V. Kuncser, G. Filoti, Sol. State Ionn 176 (2005) 97.